Photoacoustic Imaging for Cancer Diagnosis

Toshihiro Kushibiki and Miya Ishihara*

Department of Medical Engineering, National Defense Medical College, Japan

Abstract: Photoacoustic imaging (PAI) is a unique modality that overcomes the resolution and depth limitations of optical imaging of tissues while maintaining relatively high contrast. In this article, we review the biomedical applications of PAI, assisted or unassisted by exogenous photoabsorbers (contrast agents). Representative endogenous contrast agents include melanin and hemoglobin, whereas exogenous contrast agents include dyes, metal nanoparticles, and other constructs that absorb strongly in the near-infrared band of the optical spectrum and generate strong photoacoustic responses. These contrast agents, which can be specifically targeted to molecules or cells, have been coupled with photoacoustic imaging for preclinical and clinical applications including detection of cancer cells, sentinel lymph nodes, micrometastases, and monitoring of angiogenesis. Multi-functional agents have also been developed that can carry medicines or simultaneously provide contrast in multiple imaging modalities. Furthermore, contrast agents are used to guide and monitor therapeutic procedures. Overall, photoacoustic imaging has significant potential to assist in diagnosis, therapeutic planning, and monitoring of treatment outcome for cancers and other pathologies.

Keywords: Photoacoustic imaging (PAI), cancer, contrast agents, melanin, hemoglobin, gold nanomaterials.

INTRODUCTION

To develop successful therapeutic strategies against cancers and prevent tumors from recurring, it is essential to thoroughly characterize the structural, functional, and metabolic properties of tumors. The research efforts devoted toward this goal are not limited to development of new treatments and discovering the root causes of diseases, but also include development of imaging technologies that can aid in early detection of cancers and provide comprehensive real-time information regarding tumor properties. Currently, ultrasound imaging (USI), magnetic resonance imaging (MRI), X-ray computed tomography (CT), and nuclear imaging techniques like positron emission tomography (PET), and single-photon emission computed tomography (SPECT) are being used to detect tumors in patients [1-3]. With the development of various targeted contrast agents, these imaging techniques are also able to provide molecular information about malignant tumor tissues. However, optical-microscopic imaging techniques have higher resolution (0.1 mm) than USI (1 mm), MRI (1 mm), CT (1 mm), PET (8 mm), and SPECT (12 mm), and can detect a smaller number of cancer cells [4]. The need for an imaging technique that can provide high–optical contrast images at microscale resolution and reasonable penetration depth has now been met by photoacoustic imaging (PAI) [5], also known as optoacoustic imaging.

*Address correspondence to this author at the Department of Medical Engineering, National Defense Medical College, 3-2 Namiki, Tokorozawa, Saitama 359-8513, Japan; Tel: +81-4-2995-1211; Fax: +81-4-2996-5199; E-mail: miyaishi@ndmc.ac.jp

In pre-clinical studies, PAI can visualize tumor locations deep within a tissue, and is also able to provide information about tumor vasculature and hemoglobin oxygen saturation [6] and monitor angiogenesis [7]. Another advantage of PAI is its compatibility with widely available USI techniques [8]; when combined, PAI and USI can simultaneously provide anatomical and functional information about tumors. Hence, PAI has shown tremendous potential to simultaneously provide structural, functional, and molecular information.

When a short-pulse laser irradiates biological tissues, wideband ultrasonic waves (referred to as photoacoustic waves) are induced as a result of transient thermoelastic expansion. The magnitude of the photoacoustic (PA) waves is proportional to the local optical-energy deposition; hence, the waves divulge physiologically specific optical absorption contrasts. Because optical-energy deposition is related to the optical absorption coefficients of pigments, concentrations of multiple pigments can be quantified for functional imaging by varying the laser wavelength. Because ultrasonic scattering is two to three orders of magnitude weaker than optical scattering in biological tissues, ultrasonic imaging can provide better spatial resolution than pure optical imaging when the imaging depth is larger than one optical transport mean-free-path (~1 mm). For the same reason, PA sources can be localized with high spatial resolution below ~1 mm using a high-frequency focused ultrasonic transducer. The ultrasound wave is detected by a transducer that converts the mechanical acoustic waves to electric signals, and the captured signals are then processed to form an image [9]. A typical PAI setup consists of two main components: a laser (generally a tunable

ISSN: 1927-7210 / E-ISSN: 1927-7229/13

nanosecond pulsed laser) and a USI system. Most ultrasound image-processing techniques translate directly to PAI. Other reviews have provided detailed information regarding the equations governing the PA effect, various PA system configurations, and the image-processing algorithms [9, 10].

Optical absorption changes as a function of wavelength for a variety of endogenous chromophores, including melanin, oxy-(HbO_2), and deoxy-hemoglobin (Hb). The spectroscopic or multi-wavelength imaging techniques are used to characterize optical properties of tumor tissue. For example, HbO_2 and Hb have different wavelength-dependent optical absorption properties, which allows spectroscopic PAI to differentiate between arteries and veins. Furthermore, HbO_2 and Hb have the same optical absorption (~805 nm); therefore, PAI at this and other wavelengths can be used to assess total hemoglobin and blood oxygenation. PA contrast can also be enhanced by exogenous contrast agents (e.g. dyes or nanoparticles) that have distinct and tunable absorption spectra in the near-infrared (NIR) optical window (600–1100 nm), where endogenous chromophores such as hemoglobin and water have low absorption. In this review article, we summarize recent reports regarding cancer detection by PAI with endogenous contrast and exogenous contrast agents.

Cancer Detection with Endogenous PA Contrast

Cancer detection using PAI with endogenous chromophores is an area of active research. For example, PAI has been used to monitor melanoma tumor growth over the course of two weeks, with optical contrast provided by a higher concentration of melanin in the tumor relative to the surrounding tissue [11]. PAI has also been used to detect skin melanoma [6, 11-18]. Those studies indicate that PAI has the potential to identify, visualize, and track tumors and their associated vasculature at high resolution.

Using the natural contrast provided by high melanin concentrations in melanoma, PA can be used to monitor the presence of tumor cells in lymph nodes. For example, one group developed a PA method that probes entire intact nodes by placing three piezoelectric acoustic detectors near the lymph node to detect PA pulses generated within it [14]. When as few as 500 melanoma cells were injected into the tissue, a PA response could be detected, whereas control (i.e., normal) lymph nodes exhibited no response. Thus, PA generation allows detection of melanoma micrometastases in sentinel lymph nodes, potentially guiding further histologic study of tumor-proximal nodes and increasing the overall accuracy of sentinel lymph-node biopsies.

Micrometastases in lymph nodes could also be evaluated using PA tomography (PAT). Such a technique was first applied to the *ex vivo* multi-wavelength imaging of pig lymph nodes into which melanoma cells had been introduced to simulate micrometastases [17]. Based their experiences with this animal model, the authors then proceeded with imaging of a suspect human lymph node, and validated the PAI results by comparing a reconstructed slice with a histopathological section through the node. In another study of the applicability of PA tomographic imaging as an intraoperative modality for examining resected lymph nodes, six suspect lymph nodes from patients undergoing lymphadectomy for metastatic melanoma were subjected to multiple-wavelength PA [18]. Histopathological examinations revealed that three of the nodes contained melanoma cells (malignant nodes), whereas three lacked tumor cells (benign nodes). The resulting PA images were compared with histological and anatomical features, revealing that multiple areas containing melanoma cells could be identified due to the distinct imaging behavior of the tumor cells: malignant nodes exhibited higher PA responses than benign nodes, and responded differently to increases in excitation wavelength. Furthermore, anatomical differences between the two classes of nodes could be detected. In the future, the developers of this technique plan to improve specificity by implementing an adjusted illumination scheme and introducing depth correction for photon fluence. Together, the results obtained to date using PAT indicate that it has the potential to develop into an intraoperative imaging modality that could be used to detect melanoma metastases of resected sentinel lymph nodes.

Another critical stage of metastasis, the movement of tumor cells through the circulatory system, can also be monitored by PA *via* exploitation of the endogenous thermoelastic properties of melanoma cells [13]. In this method, PA excitation is coupled with a detection system capable of determining the presence of disseminating cells within the blood *in vitro*. Based on the results to date, this approach could enable clinicians to assay healthy and metastatic patients for the presence of migrating melanoma cells using simple blood draws, an unprecedentedly powerful method for routine cancer screening.

Endogenous PA contrast has also been used to image cells at extremely high resolution *via* PA microscopy (PAM). By taking advantage of the properties of fluorescent and nonfluorescent endogenous pigments, *in vivo* subwavelength-resolution PAM (SW-PAM) has been developed [15]. SW-PAM provides exquisitely high optical-absorption contrast at an optical resolution approaching the ultimate diffraction limit, and is thus capable of resolving subcellular organelles. In conjunction with scaled-up macroscopy, the only technology capable of measuring the same contrast origin over such wide length scales, SW-PAM could potentially accelerate translation from fundamental microscopic research to clinical applications. PAM has also been used to monitor melanoma cells inside three-dimensional (3D) porous scaffolds more than 1 mm thick, with the specific goal of evaluating the effects of seeding and culture on spatial distribution and temporal proliferation [16]. In that study, PAM imaging could successfully resolve the spatial distribution of cells within the scaffold, and the concomitantly obtained volumetric information allowed quantitative assessment of the number of cells in the scaffold, which was validated by MTT assay.

PAM can also be used *in vivo*, as now demonstrated in multiple animal-model studies. In nude mice, dual-wavelength reflection-mode PAM has been used to non-invasively obtain 3D images of subcutaneous melanomas and their surrounding vasculature in living animals [12]. Reflection-mode PAM was has also been used to monitor melanoma cells growing in the brain, a model of metastatic melanoma [11]. In that study, melanoma cells were implanted in the brain of a mouse, and PAM was used to scan the region of implantation over time and monitor tumor growth until the death of the animal. The results demonstrated that PAM can noninvasively detect and monitor growth of melanoma in the brain of a living organism.

The use of melanin as an endogenous contrast agent may be limited to studies of melanoma, but other features are more widely shared among types of cancer. In particular, compared to normal tissue, malignant tumors have dense and unorganized vasculature. From this viewpoint, it has been possible to use endogenous hemoglobin–based PA to assess multiple tumor types. PA also enables *in vivo* label-free functional imaging of hemoglobin oxygen saturation (sO_2) in vessels down to single capillaries of mouse ear (Figure **1**) [19]. The high density of blood vessels in tumors enhances PA image contrast, due to the properties of endogenous hemoglobin, thereby enabling tumor detection [6, 7, 20-25]. For example, PAI was used to monitor tumor neovascularization following subcutaneous inoculation of pancreatic tumor cells into rats [7]. The images, collected over a 10 day period, were obtained from ultrasound generated by absorption of short laser pulses (1064 nm wavelength) by hemoglobin. The resulting 3D data allowed visualization of blood vessel development, as well as quantification of the extent of individual tumor-proximal blood vessels, blood concentration changes within the tumor, and growth in the depth of the neovascularized region.

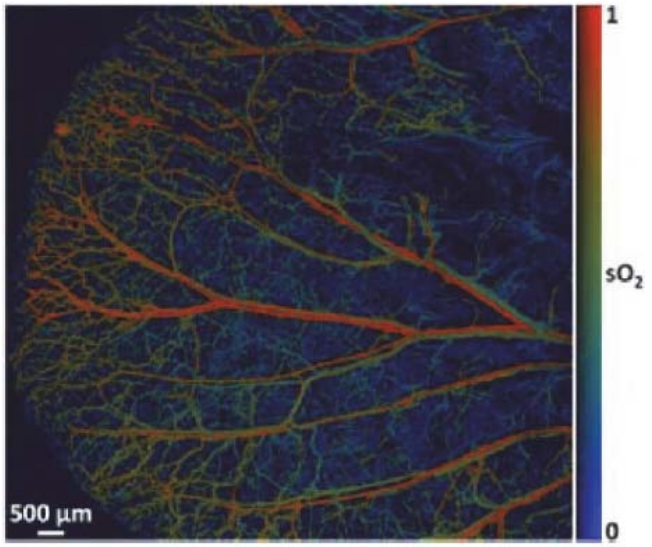

Figure 1: With dual-wavelength measurements (561 nm and 570 nm), PAM can also reveal the hemoglobin oxygen saturation (sO_2) of the whole-ear vasculature at the capillary level. Adapted with permission from [19]. Copyright (2011): The Optical Society of America.

In a mouse model of breast cancer, PAI was used to monitor the progress of vascularization during early tumor growth [20]. Measurements were taken over a 20 day period following subcutaneous inoculation of breast cancer cells into mice. In the PA images, the morphology of the tumor proximal vasculature was clearly resolved, allowing changes in structure and increases in vessel density to be unambiguously identified. Furthermore, the average PA signal strength of the vasculature in the tumor region, which is highly correlated with the total blood hemoglobin concentration, was enhanced during the early stages of tumor growth. Thus, it should be feasible to use PAI to detect early-stage tumors and monitor the progress of anti-angiogenic therapy. Another animal-model study explored the feasibility of PAT for noninvasive imaging

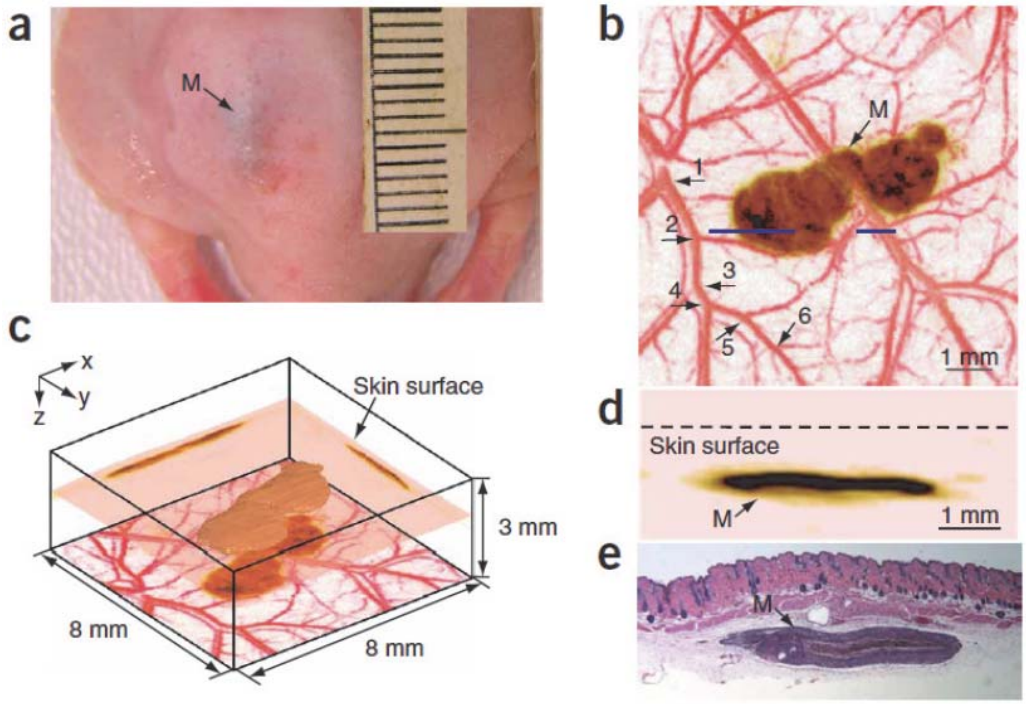

Figure 2: *In vivo* imaging of a subcutaneously inoculated B16-melanoma in a nude mouse using fPAM at 584 nm and 764 nm. (**a**) Photograph of the melanoma. (**b**) A composite of the two maximum amplitude projection (MAP) images projected along the z axis, where an MAP image is formed by projecting the maximum photoacoustic amplitudes along a direction to its orthogonal plane. Here, blood vessels are pseudocolored red in the 584 nm image and the melanoma is pseudo-colored brown in the 764 nm image. As many as six orders of vessel branching can be observed in the image as indicated by numbers 1–6. (**c**) Three dimensional rendering of the melanoma from the data acquired at 764 nm. Two MAP images at this wavelength projected along the x and y axes are shown on the two side walls, respectively. The composite image shown in a is redrawn at the bottom. The top surface of the tumor is 0.32 mm below the skin surface, and the thickness of the melanoma is 0.3 mm. (**d**) An enlarged cross-sectional (B-scan) image of the melanoma parallel with the z-x plane at the location marked with a dashed line in a. (**e**) Hematoxylin and eosin (HE) stained section at the same marked location. M, melanoma.

Adapted with permission from [6]. Copyright (2006): Nature Publishing Group.

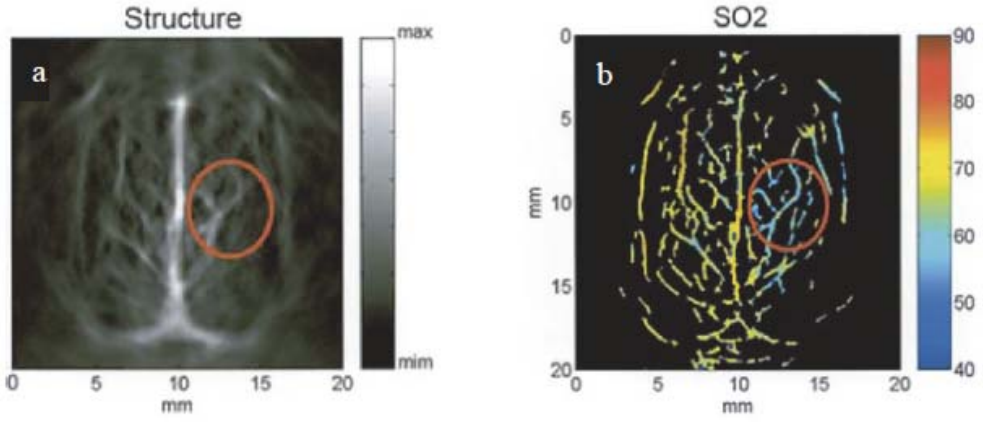

Figure 3: Estimated brain blood oxygen saturation image from noninvasive *in vivo* photoacoustic tomography (PAT) of an SD rat brain at three weeks post inoculation with ENU1564 cells. The circle indicates the position of the tumor. (**a**) PAT image of the rat brain inoculated intracranially with ENU1564 cells and reveals the vascular architecture associated with the tumor. (**b**) Estimated brain blood oxygen saturation (sO2) image.

Adapted with permission from [27]. Copyright (2007): Spandidos Publications.

of prostate cancer [22]. Using a commercially available medical ultrasound (US) system, it was possible to image blood-rich lesions simulating prostate tumors *in vivo* in dogs. Based on the optical contrast between hemoglobin and other tissues, PAT demonstrated high sensitivity and contrast-to-noise ratio. Notably, because this method did not compromise the originally designed imaging functions of the instrument, simultaneously

obtained US images revealed morphological features such as the boundary between the urethra and the prostate. Further evidence that PA will be useful in a clinical context is provided by a study of PA mammography in diagnosis of breast cancer, including an evaluation of therapeutic responses relative to other diagnostic modalities [25]. Using a prototype PA mammography instrument, 27 breasttumor lesions were measured, including 21 invasive breast cancers (IBC), five ductal carcinomas in situ (DCIS), and one phyllodes tumor. The resulting PAM images were comparable to those obtained by magnetic resonance imaging (MRI). Based on these findings in breast and prostate cancers, it is clear that the ability of PAM to measure tumor vascularity and oxygenation demonstrate that this method will be useful for diagnosis and characterization of multiple tumor types.

The potential resolution of hemoglobin-based methods is quite high, as illustrated by multiple PAM studies. Compared to other vascular imaging techniques, including dynamic-enhanced MRI, CT perfusion, and functional PET [26], PAI detects tumor vasculature at comparable or higher resolution, without the use of exogenous contrast agents. One good example is simultaneous imaging of melanomas and hemoglobin. At 584 nm, functional PAM (fPAM) can image the morphological relationship between a melanoma and the surrounding blood vessels in the x-y view, because both melanin and hemoglobin have similarly strong absorptions at this wavelength. However, visible light at this wavelength is not suitable for measuring tumor thickness, because it cannot easily penetrate the melanin-rich tumor. This limitation can be overcome, however, by generating another image using 764 nm NIR light, which can infiltrate the tumor because of both the decreased optical absorption of melanin and the minimal optical absorption of blood. Combining the two images from these two spectral regions reveals the 3D morphology of both the melanoma and the surrounding vasculature (Figure **2**) [6]. Microvessels with diameters of less than a single pixel (50 mm), presumably resulting from angiogenesis, can be seen surrounding the melanoma (Figure **2b**). This demonstrates that fPAM can potentially detect and evaluate melanomas and microvasculature. fPAM provides multiple-wavelength imaging of optical absorption and permits high spatial resolution at depth, with a ratio of maximum imaging depth to depth resolution greater than 100 [6]. Another proposed method, label-free metabolic PAM (mPAM), can noninvasively quantify the rate of oxygen metabolism (MRO_2) in absolute units at small-vessel resolution *in vivo* [24]. Using this method, it was shown that increased MRO_2 does not necessarily cause hyperoxia or increase oxygen extraction; instead, early-stage cancers were shown to be hyperoxic despite their hypermetabolism of oxygen. mPAM has also been used to longitudinally image hyperthermia, cryotherapy, melanoma, and glioblastoma *in vivo*. Beyond imaging melanin and blood vessels, PAI systems have also been employed to measure the oxygen content of blood in studies of hypoxia in tumors [27]. Hypoxia is often linked to malignancy and resistance to therapy. The sO_2 in the blood can be estimated by comparing the PA signal strengths of HbO_2 and Hb obtained from spectroscopic PA images (Figure **3**). Li *et al*. performed *in vivo* functional imaging of a mouse brain with a glioblastoma, and demonstrated that a hypoxic region indicated the location of the tumor in the brain [28]. Their results clearly show that the tumor has a lower percentage sO_2 than the surrounding normal tissue.

Cancer Detection with Exogenous PA Contrast Agents

The sensitivity of the PAI technique in imaging deeply situated tumors can be dramatically increased by utilizing exogenous contrast agents. Representative exogenous contrast agents used for detecting tumors were listed in Table **1**. NIR-absorbing dyes, such as Alexa Fluor [29, 30] and indocyanine green (ICG) [31-37], have been used to enhance PA contrast. Both of these dyes conjugated with antibody have proven useful for detection of HER2-positive breast-cancer cells. *In vitro* PAT imaging revealed the specificity of Herceptin antibodies labeled with Alexa Fluor–750: in HER2-positive cell lines, PA signal intensity gradually increased as a function of cell number, whereas in HER2-negative cells lines, PA signal was not detectable above baseline [30]. HER-2 antibodies have also been conjugated to nanoparticles containing ICG [32]. These nanoparticles, which are more stable in solution than free ICG dye, were developed as a contrast agent for PAI based on PEBBLE (Photonic Explorers for Biological use by Biologically Localized Embedding) technology, using organically modified silicate as a matrix. ICG has also been incorporated into polymer-based degradable nanoparticles with NIR absorption suitable for PAI; the high optical absorption at a relevant NIR wavelength (800 nm), coupled with an absence of cytotoxicity, makes these nanoparticles promising candidates for degradable PA contrast agents [34]. When conjugated with HER-2 antibody,

Table 1: Representative Exogenous Contrast Agents Used for Detecting Tumors by Photoacoustic Imaging

Contrast agent	Observation	Ref
Alexa Fluor–750	Labeled Herceptin antibody for noninvasive assessment of HER2 expression.	[30]
ICG	Incorporated in nanoparticles with HER2 antibody for breast and prostate cancer cell targeting.	[32]
	Sentinel lymph nodes and lymphatic vessels mapping.	[33]
	Incorporated PLGA nanoparticles for exhibiting the absorption suitable for imaging.	[34]
	Encapsulated in the emulsion to monitor the ultrasound initiated drug delivery.	[35]
ICG + carbon nanotubes	Sentinel lymph nodes and urinary bladder mapping.	[36]
	ICG enhanced single walled carbon nanotubes were conjugated as the contrast agent with cyclic Arg-Gly-Asp (RGD) peptides to molecularly target integrins.	[40]
Gold nanorods	Detection of the endocytosed gold nanorods in cells or in vivo tumors	[39, 66, 68]
	Multiple targeting by utilizing the tunable optical absorption property of gold nanorods. HER2 and EGFR targeted.	[42]
	Conjugated with anti-ICAM-1 antibody or anti-E-selectin were exposed to HUVECs with different stimulation conditions to monitor the upregulation of these molecules.	[48]
	Combined intravascular ultrasound and intravascular photoacoutic imaging of atherosclerotic rabbit aortas following systemic injection of gold nanorods was established.	[50]
	The combination of nanorods and high intensity focused ultrasound for imaging and treatment (ablation) of solid tumor.	[57]
	A novel technique based on gold nanorods for quantitatively monitoring focused-ultrasound induced blood-brain barrier (BBB) opening.	[59]
	Silica-coated gold nanorods were evaluated for novel contrast agents.	[60-63]
	Incorporated gold nanorods into the core of self-assembled lipid-encapsulated nanoparticles.	[64]
	Modified with the antibodies infliximab and certolizumab for targeting TNF-alpha to detect inflammation in arthritic mouse knees.	[67]
	Quantitation of the number of mesenchymal stem cells uptake silica coated gold nanorods after injection to the muscle tissue.	[69]
	Gadolinium(III)-gold nanorods have been developed as a dual-modality probe for MRI and PAI to trace macrophages for determining the degree of inflammation	[72]
Gold nanocages	Evaluation of the melanoma imaging by the gold nanocages conjugated with [Nle(4),D-Phe(7)]- alpha-melanocyte-stimulating hormone.	[41]
	The lymph node tracers for noninvasive imaging of sentinel lymph nodes.	[52, 53]
	The hollow interiors of gold nanocages with a phase-change material (PCM) that has a melting point of 38-39 degrees C. When exposed to direct heating or high-intensity focused ultrasound, the PCM melt and escape from the interiors of nanocages through small pores on the surface, concurrently releasing the encapsulated molecules into the surrounding medium.	[58]
Gold nanoparticles	Gold nanoparticles targeting EGFR via antibody, leading to a red shift in their plasmon resonance frequency.	[43, 47]
	To detect macrophages in atherosclerotic plaques, plasmonic gold nanoparticles are introduced as a contrast agent for intravascular imaging.	[49]
	To assess the intravenous delivery of hollow gold nanospheres targeted to integrins overexpressed in both glioma and angiogenic blood vessels.	[55]
PEGylated gold nanoparticles	Accumulation of PEGylated gold nanoparticles in tumors was effectively imaged.	[45]
Gold nanoshells	The conjugation of gold nanoshells displaying near-infrared absorption properties for imaging with VCAM-1 antibody molecules and PEG to increase their biocompatibility.	[51]
Hollow gold nanospheres	The imaging of brain vasculature with high spatial resolution and enhanced sensitivity.	[56]
Carbon nanotubes	Single-walled carbon nanotubes (SWNTs) conjugated with cyclic Arg-Gly-Asp (RGD) peptides as a contrast agent for PAI of tumors.	[71]
	SWNTs have been used to map SLNs as well as the urinary bladder, demonstrating that dye-conjugated SWNTs might be used to identify SLNs in breast cancer patients.	[75, 76]
	Enhance the imaging contrast of multipotent marrow stromal cells after uptaking carbon nanotubes and synergistically enhanced the stimulation of osteogenesis differentiation.	[77]

ICG-embedded PEBBLEs exhibited high-contrast and high-efficiency binding to prostate-cancer cells [34]. Together, these results indicate that PAT- and PAI-based measurement of NIR dye–conjugated antibodies is a feasible approach.

As a representative NIR dye, ICG has been employed in multiple studies to map sentinel lymph nodes (SLN). In dual-modality volumetric-spectroscopic PAI in rats, SLNs and lymphatic vessels were clearly visible [33]. The feasibility of mapping SLNs, as well as the urinary bladder, was also demonstrated using single-walled carbon nanotubes (SWNTs) as a nonionizing PA contrast agent [36]. To improve the PA sensitivity, the SWNTs were conjugated to ICG. *In vivo* PA imaging results revealed clear visualization of SLN and bladder due to accumulation of ICG-SWNTs. Such ICG-SWNTs could be potentially utilized in combination with PA imaging to identify SLNs in breast cancer patients and track the vesicoureteral reflux. More generally, in conjunction with ICG, PAI has the potential to help map SLNs in axillary staging, and to help evaluate tumor metastasis in patients with breast cancer.

The utility of ICG is not limited to its function as a dye: ICG has other properties that could be useful not only in visualization of tumors, but also in their treatment. Because ICG generates toxic oxygen upon illumination at specific wavelengths, it could be useful as a photosensitizer for photodynamic therapy; one study, also referenced above, has measured the photosensitization capability of ICG-embedded silicate nanoparticles [32].

An interesting recent advance in PAI is the use of photo-activable probes to provide a target-dependent PA signal. These probes exhibit superior specificity and sensitivity relative to probes that do not interact with the target. For example, photo-activable probes have been designed to specifically target matrix metalloprotease 2 (MMP-2), a protease that is overexpressed in many aggressive cancers [38]. The probe's peptide platform consists of a cell-penetrating peptide that is recognizable by MMP-2 both *in vitro* and in mouse models. Before cleavage by MMP-2, the intact probe yields PA signals of similar intensity at the two wavelengths corresponding to the absorption maxima of the chromophores BHQ3 (675 nm) and Alexa Fluor 750 (750 nm). When the probe is cleaved by the appropriate enzyme, the BHQ3 dye associated with the cell penetrating peptide (CPP) portion of the probe accumulates in nearby cells, whereas the Alexa dye diffuses away, resulting in a PA signal visible only at 675 nm [38].

Among the exogenous contrast agents, gold materials have attracted attention in the context of nanoparticle-based PAI, due to their unique optical properties arising from the surface plasmon resonance (SPR) effect. Because of the SPR effect, gold materials have absorbances that are orders of magnitude higher than those of NIR dyes. For example, gold nanospheres, nanorods, nanoshells, nanocages, and nanobeacons have been used in PAI because of their tunable and strong longitudinal plasmon resonance in NIR wavelengths. Noninvasive PAM has been developed to image intracellular gold nanorods (AuNRs) with high optical-absorption contrast [39]. In that study, AuNRs were taken up by MCF7 cells and could be imaged using a PAM system developed in-house by the research group. Successful intracellular monitoring of the AuNRs revealed their time-dependent uptake and distribution within cells. The results demonstrated that PAM can be applied in a complementary manner to imaging of nonfluorescent particles, powerfully combining *in vivo* microscopy and nano-bio methods.

Attachment of targeting moieties to exogenous agents makes it possible to obtain specific molecular information about tumors. Gold materials with different optical absorption properties can be conjugated to cancer-specific biomarkers, such as growth-factor receptors and integrins [40-45]. By utilizing multiple targeted gold materials, multiplex molecular labeling of a tumor can be achieved, and multi-wavelength PAI can image the heterogeneous accumulation of gold materials with cancer cells *in vivo*. Fluorescent optical probes, such as quantum dots, also provide PA contrast and can be used for multiplex labeling of tumors [46].

Molecule-specific detection using gold-containing materials is exemplified by studies in which gold nanoparticles were used to target cells expressing EGFR. Gold nanoparticles labeled with anti-EGFR antibodies have been shown to undergo aggregation when they bind EGFR on cell surfaces, leading to a red shift in their plasmon resonance frequency (Figure **4**) [43]. Capitalizing on that effect, the authors of that study used subcutaneous tumor-mimicking gelatin implants in *ex vivo* mouse tissue to evaluate the efficacy of a molecularly specific PAI technique. Another study using gold nanoparticles functionalized with antibodies showed that these agents can

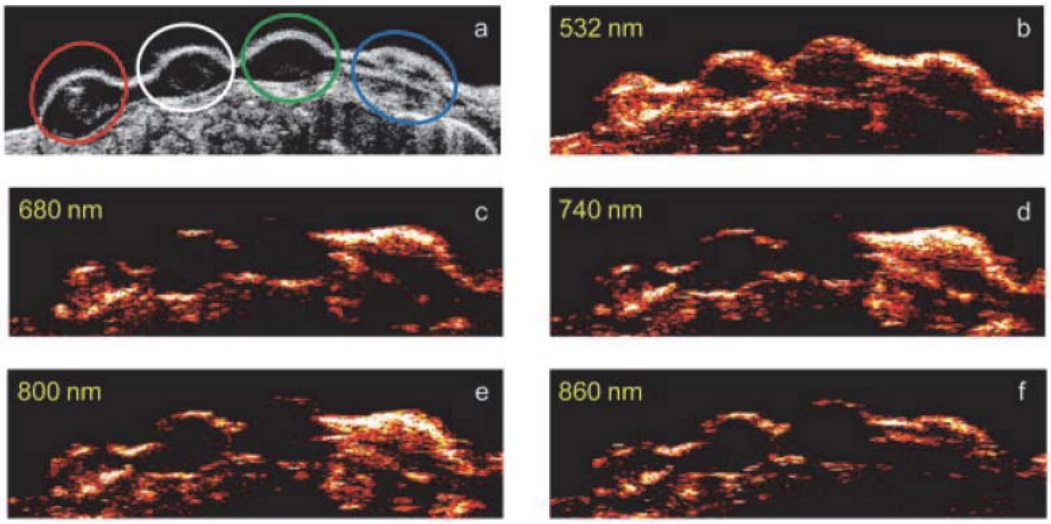

Figure 4: The ultrasound (**a**) and photoacoustic images (**b-f**) obtained at multiple wavelengths (532, 680, 740, 800, and 860 nm). The ultrasound image clearly shows the mouse skin as the hyperechoic region and the subcutaneous gelatin implants as the hypoechoic regions. The regions of gelatin implant with EGFR targeted AuNPs, PEGylated AuNPs, control A431 cells, and the ADS740WS dye are encircled in red, green, white, and blue insets, respectively. As expected, the gelatin implant with control A431 cells (white inset) does not produce any photoacoustic signal while the cells mixed with PEGylated AuNPs (green inset) produce photoacoustic signal only at 532 nm laser irradiation. The intensity of the photoacoustic transients produced by the cells labeled with EGFR targeted AuNPs (red inset) decreases as a function of wavelength in congruence with the optical absorption properties of these cells. The photoacoustic image at 740 nm (**d**) clearly has greater photoacoustic signal intensity in the region of the gelatin implant with dye. Indeed, the ADS740WS dye used as a pseudo control has an absorption peak at 740 nm. Therefore, the multiwavelength photoacoustic images qualitatively indicate the spectral variations in the optical absorption properties of the gelatin implants. The images measure 44 mm laterally and 11 mm axially.
Adapted with permission from [43]. Copyright (2009): American Chemical Society.

specifically bind to molecular biomarkers such as EGFR [47]. In that study, PAI was performed with 532 and 680 nm pulsed-laser irradiation on 3D tissue phantoms created using a human keratinocyte cell line. The results of these two studies demonstrate that the use of multi-wavelength PAI and molecularly targeted (anti-EGFR) gold nanoparticles makes possible highly sensitive and selective detection of cancer cells.

Molecular targeting of gold-containing nanoparticles can be directed at more than one molecule at the same time. Using the tunable optical absorption property of AuNRs, these materials have been used for simultaneous multiple targeting for PA molecular imaging [42]. This technique allows multiple molecular signatures to be obtained by simply switching laser wavelength. In the proof-of-concept study, HER2 and EGFR were chosen as the primary target molecules in two types of cancer cells; based on both *in vitro* and *in vivo* mouse model imaging experiments, the potential of this technique to improve cancer diagnosis was demonstrated. In an exclusively *in vitro* study, the upregulation of intercellular adhesion molecule-1 (ICAM-1) and E-selectin were simultaneously detected by PA molecular imaging (PMI) [48]. AuNRs conjugated to either anti-ICAM-1 antibody or anti-E-selectin were exposed to HUVECs under different stimulation conditions. For both ICAM-1 and E-selectin, the averaged PA signal intensities from the stimulated cells were about 3-fold higher than those of un-stimulated cells. Strong binding of AuNRs to the stimulated HUVECs was demonstrated by fluorescence imaging.

Beyond cancer and angiogenesis, gold-containing nanoparticles have also been employed in the study of other diseases, especially atherosclerosis. For example, to detect macrophages in atherosclerotic plaques, plasmonic gold nanoparticles were introduced as a contrast agent for intravascular PAI [49]. Phantom and *ex vivo* tissue studies suggested that intravascular PAI could assess the macrophage-mediated aggregation of nanoparticles and therefore identify the presence and the location of nanoparticles associated with macrophage-rich atherosclerotic plaques. Previously, combined intravascular ultrasound and intravascular PA (IVUS/IVPA) imaging has been established as a viable means for assessing atherosclerotic plaque morphology and composition using both endogenous and exogenous contrast. Those findings were extended by a study in which IVUS/IVPA imaging was performed on atherosclerotic rabbit aortas following systemic injection of AuNRs with peak absorbance within the tissue optical window [50],

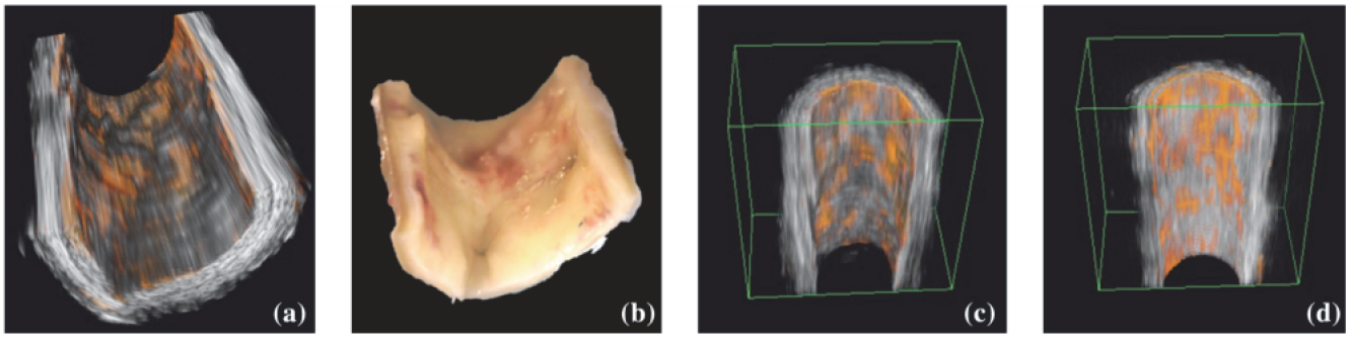

Figure 5: Three-dimensional integrated intravascular ultrasound and intravascular photoacoustic (IVUS/IVPA) renderings of gold nanorod (AuNR)-labeled atherosclerotic plaque. Fixed sections of a balloon injured New Zealand white rabbit aorta were subsequently imaged using the integrated IVUS/IVPA catheter. (**a**) Combined IVUS/IVPA rendering of an 8-mm long section of atherosclerotic rabbit artery obtained through saline. (**b**) Photograph of the corresponding artery section revealing AUNR distribution at the luminal surface (red). Combined IVUS/IVPA images obtained through saline (**c**), and through blood (**d**) of aseparate 6-mm arterial section. Step size, 500 μm.

Adapted with permission from [50]. Copyright (2012): SPIE.

demonstrating that AuNR detection within the arterial wall can be achieved using IVUS and PAI, even in the case of imaging through luminal blood (Figure **5**). In another study, a PA molecular probe based on gold nanoshells was targeted to VCAM-1 in mice using specific antibodies [51]. These immune-nanoshells were nontoxic, biocompatible, and could be distinguished from blood both *in vitro* and *in vivo* by PAT. Optical projection tomography revealed that the immunonanoshells accumulated in atherosclerosis-prone regions. Such technologies could be used in the clinic to target atherosclerotic plaques and monitor or deliver therapies to these sites.

Gold nanocages (AuNCs) have been demonstrated to be a new class of lymph node tracers for noninvasive PAI of SLNs in an animal study that showed the AuNCs could be detected by PAI as deep as 33 mm below the skin [52]. Most importantly, in contrast to methylene blue, AuNCs can be easily bioconjugated with antibodies for targeting specific receptors, potentially eliminating the need for invasive axillary staging procedures in addition to providing noninvasive SLN mapping. Support for this idea was provided by a systematic investigation of the use of AuNCs as a novel class of optical tracers for noninvasive SLN imaging by PAT in a rat model [53]. The transport of AuNCs in a lymphatic system and uptake by the SLN were evaluated using PAT in the axillary region of rats. Quantification of AuNCs accumulated in the lymph node was achieved by correlating the data from PAI with the results from inductively coupled plasma mass spectrometry. These results are critical to the further development of this AuNC-based PA tomography system for noninvasive SLN imaging, providing valuable information for metastatic cancer staging. SLNs have also been detected in NIR wavelengths using gold nanobeacons (AuNBs) to provide PA contrast in a rodent model [54]. That study revealed that size dictates the *in vivo* characteristics of these nanoparticles: larger AuNBs with large gold payloads were not as efficient as smaller AuNBs for this purpose. Smaller AuNBs were observed to traffic through the lymphatic system and accumulate more efficiently in the lymph nodes, in comparison to larger nanoagents. Their results showed that cumulative nanoparticle deposition in lymph nodes is size-dependent, and that high payloads of gold, although offering greater contrast *in vitro*, may yield nanoagents with poor intradermal migration and lymphatic transport characteristics.

A growing body of research has focused on the use of gold nanoparticles in the context of PAT. PAT has been used to assess the intravenous delivery of hollow gold nanospheres targeted to integrins that are overexpressed in both glioma and angiogenic blood vessels in a mouse model of glioma [55]. In that study, photothermal ablation (PTA) treatment significantly prolonged the survival of tumor-bearing mice. Furthermore, evaluation of the ability of systemically administered PEGylated gold particles to serve as a contrast agent for *in vivo* tumor imaging revealed that subcutaneously administered nanoparticles can be visualized in mice using PAT [45]. In tumor-bearing mice, such nanoparticles can also be effectively imaged in tumors. Thus, PAT using gold nanoparticles as a contrast agent has important potential applications in image-guided therapy of superficial tumors. Their utility can be further enhanced by molecular targeting: when bioconjugated with [Nle(4),D-Phe(7)]-alpha-melanocyte-stimulating hormone, AuNCs can serve as

a novel contrast agent for *in vivo* molecular PAT of melanomas, and these agents have both exquisite sensitivity and high specificity [41]. Bioconjugated AuNCs enhanced contrast approximately 300% above that of control, PEGylated AuNCs. That study also validated the *in vivo* PAT quantification of the amount of AuNCs accumulated in melanomas. PAT has also been used in conjunction with a new class of optical contrast agents based on mesoscopic hollow gold nanospheres (HAuNS) [56]. PAT images acquired within 2 h after intravenous administration of PEG-HAuNS to nude mice revealed the brain vasculature with greater clarity and detail than PAT images based on intrinsic optical contrast. No acute toxicity to the liver, spleen, or kidneys was observed following a single imaging dose of PEG-HAuNS. Thus, due to their high spatial resolution and enhanced sensitivity, PEG-HAuNS are promising contrast agents for PAT.

The combination of gold-containing materials with ultrasound techniques is a particularly active focus of research and development of the potential for gold as a component of therapies. In a study intended to demonstrate the feasibility of combined contrast imaging and treatment of a solid tumor *in vivo* using an integrated PAI and high-intensity focused ultrasound (HIFU) system, the tumor was clearly visible on PA images after the injection of AuNRs, and HIFU was able to ablate the tumor under the guidance of PAI [57]. Another report describes a new theranostic system with a combination of capabilities aimed at both enhancing the contrast of PMI and controlling the release of a chemical or biological effector by HIFU [58]. The fabrication of this system involves filling the hollow interiors of AuNCs with a phase-change material (PCM) that has a melting point of 38–39°C. The PCM can be premixed and thus loaded with a dye, as well as other chemical or biological effectors. When exposed to direct heating or HIFU, the PCM will melt and escape from the interiors of AuNCs through small pores on the surface, concurrently releasing the encapsulated molecules into the surrounding medium. The release profile can be controlled by varying the power of HIFU, the duration of exposure to HIFU, or both. A novel PAI technique, based on AuNRs for quantitatively monitoring focused-ultrasound (FUS) induced blood-brain barrier (BBB) opening in a rat model *in vivo,* takes advantage of the strong NIR absorption of AuNRs; furthermore, due to their small size, AuNRs tend to extravasate from BBB opening foci, resulting in passive labeling of the BBB disruption area [59]. The results showed that AuNR contrast-enhanced PAM successfully reveals the spatial distribution and temporal response of BBB disruption areas in the rat brains. The quantitative measurement of contrast enhancement has the potential to allow estimation of the local concentration of AuNRs, and even the dosage of therapeutic molecules, when AuNRs are further used as nano-carriers for drug delivery or photothermal therapy.

Despite rapid and already extensive progress in development and application of gold-based agents, improvements in these materials are occurring continuously. Several of the most pertinent examples involve the use of silica. For example, at photon fluences typically needed for PA wave induction often also result in AuNRs shape changes that significantly reduce the efficiency of acoustic wave generation; to solve this problem, a group has proposed, synthesized, and evaluated amorphous silica–coated gold nanorods (AuNR-Si) in an effort to improve contrast agent stability and ameliorate efficiency loss during PA wave induction [60]. PA signals generated by AuNR-Si demonstrate considerably greater resistance to degradation of signal intensity with repetitive pulsing than do uncoated AuNR, thereby enabling much longer, higher-contrast imaging sessions than previously possible. The prolongation of high-contrast imaging, and biocompatibility and easy surface functionalization for targeting ligands afforded by amorphous silica, suggest AuNR-Si to be potentially significant for the clinical translation of PAT. Another group developed a multiplex PAI technique that uses targeted AuNR-Si to distinguish cell inclusions *in vitro* [61]. Cells were incubated with the targeted AuNR-Si, incorporated in a tissue phantom, and imaged using multiwavelength PAI. They used PAI and statistical correlation analysis to distinguish between the unique cell inclusions within the tissue phantom.

Silica has also been used to overcome inherent challenges arising from specific properties of gold-based contrast agents. For example, a dielectric shell has a strong influence on the amplitude of the generated PA signal, and that silica-coated AuNRs of the same optical density are capable of producing about 3-fold higher PA signals than AuNRs without silica coating [62]. These results suggest that the enhancement is caused by the reduction of the gold interfacial thermal resistance with the solvent due to the silica coating. The strong contrast enhancement in PAI, demonstrated using phantoms containing AuNR-Si, shows that these hybrid particles act as “PA

nanoamplifiers" and could potentially be used as high-efficiency contrast agents for PAI or PA image–guided therapy. Likewise, analysis of the PA signal generated by plasmonic metallic nanoparticles is complex, because of the dependence upon physical properties of both the nanoparticle and the surrounding environment. A study of the effect of the aggregation of gold nanoparticles on the PA signal amplitude revealed that the PA signal from aggregated silica-coated gold nanoparticles is greatly enhanced in comparison to disperse silica-coated gold nanoparticles [63]. Because cellular uptake and endocytosis of nanoparticles result in their aggregation, these results have important implications for the application of plasmonic metallic nanoparticles towards quantitative molecular imaging.

Strategies for improving gold nanoparticles are, of course, not limited to those involving silica. One novel approach generated self-assembled colloidal AuNRs, which are constrained to the vasculature [64]. These nanorods were incorporated into the core of self-assembled lipid-encapsulated nanoparticles (sAuNRs), providing hundreds of gold atoms per nanoparticle in a 20% colloid suspension. The physico-chemical characterization in solution and anhydrous state with analytical techniques demonstrated that the particles were spherical and highly monodisperse. In addition to describing the synthesis and characterization of this novel preparation, the authors of that study also impressively demonstrated sensitive NIR PA detection *in vitro*. In yet another approach, fluorescent nanodiamonds (FNDs) have also been combined with gold-containing materials [65]. FNDs have drawn much attention in recent years for biomedical imaging applications due to their desirable physical properties including excellent photostability, high biocompatibility, extended far-red fluorescence emission, and ease of surface functionalization. In that study, the authors observed significant enhancement of PA emission from FNDs when they were conjugated with gold nanoparticles. This new feature of FNDs that may lead to their potential application as a dual-imaging contrast agent for combined fluorescence and PAI modalities.

Among the most important purposes of gold-containing materials are the delivery of therapeutic agents and the monitoring and enhancement of therapeutic outcomes. A large body of evidence has accumulated that demonstrates the effectiveness of gold-containing materials in achieving these goals. For example, AuNRs have been used in a 3D ultrasound and PA imaging system, along with a spectroscopic PA imaging algorithm, to identify and quantify the presence of nanoparticles and other tissue constituents [66]. Using the system and approach they developed, the authors performed 3D *in vivo* imaging of a mouse with tumor before and after intravenous injection of AuNRs. Their spectroscopic PA imaging algorithm estimated distribution of nanoparticles as well as oxygen saturation of blood. The results suggested that 3D ultrasound-guided spectroscopic PA imaging can monitor nanoparticle delivery *in vivo*. In a mouse model of arthritis, AuNRs with an absorption maximum in the range of 1064 nm were modified with the antibodies infliximab and certolizumab (for targeting TNF-alpha) to detect inflammation in arthritic mouse knees [67]. The authors demonstrated an differential enhancement of PA signal amplitudes after the injection of infliximab-modified, but not certolizumab-modified or PEGylated control particles, on arthritic and healthy control mice, using a fast-scanning PAI platform based on a pulsed Nd:YAG laser and a single focused ultrasound transducer. The excellent PA properties of the AuNRs allowed confirmation of the overexpression of TNF-alpha in arthritic knees. Due to the uncomplicated coupling chemistry and the scalability of ultrasound-based imaging approaches, these results potentially allow a transfer to various preclinical and clinical applications. In a different context, i.e., ovarian-cancer screening, AuNRs were used as a passively targeted molecular imaging agent, in the first report of *in vivo* imaging of ovarian cancer tumors using PA and Raman imaging agent. [68]. AuNRs with three different aspect ratios were studied. Maximum PA signal was observed within 3 h for all cell lines tested, and increased signal persisted for at least 2 days post-administration. There was a linear relationship between the PA signal and the concentration of injected molecular imaging agent, and the same molecular imaging agent could be used for clear visualization of the margin between tumor and normal tissue and tumor debulking *via* surface-enhanced Raman spectroscopy (SERS) imaging.

Beyond degenerative disease and cancer, in the field of regenerative medicine, gold-containing materials have also been proposed means to monitor the progress and success of stem-cell therapy, where improved imaging modalities are critically needed. Techniques with real-time content to guide and quantitate cell implantation are especially important in applications such as musculoskeletal regenerative medicine. One study along these lines reported the use of silica-coated AuNRs as a contrast agent for PAI and quantitation of mesenchymal stem cells in rodent muscle tissue [69]. The silica coating increased the

uptake of gold into the cell more than 5-fold. The pluripotency of the cells was retained, and secretome analysis of a pool of 26 cytokines indicated that only IL-6 was dysregulated more than 2-fold. The low background of the technique allowed imaging of as few as 100,000 cells *in vivo*. The temporal resolution was 0.2 s, at least an order of magnitude below existing cell imaging approaches. In another study, *in vivo* and *in vitro* experiments were performed to demonstrate the efficacy of ultrasound-guided PA (US/PA) imaging to monitor mesenchymal stem cells (MSCs) labeled with gold nanotracers (AuNTs) [70]. AuNT-labeled MSCs captured in the PEGylated fibrin gel system were imaged *in vivo*, as well as *in vitro*, over a 1-week time period, demonstrating the feasibility of longitudinal cell tracking using US/PA imaging. Overall, AuNT labeling of MSCs and US/PA imaging may represent an alternative approach to stem-cell imaging that is capable of noninvasive, sensitive, quantitative, and longitudinal assessment of stem-cell behaviors, with high spatial and temporal resolutions at sufficient depths. In addition, multi-functional contrast agents were developed. Jin *et al*. reported a new generation of compact, uniform, NIR responsive magnetic nanoparticles-gold core-shell nanostructures by creating a gap between the core and shell. Not only does that approach produce a magnetically sensitive nanoparticle with both strong NIR and magnetic resonance responses, it also enables a new modality, magnetomotive photoacoustic (mmPA) imaging. Compared to PA imaging using conventional metallic nanoparticles, mmPA imaging with a coupled agent provides the same sensitivity but with markedly improved contrast specificity. Indeed, all PA signals not created by the coupled nanoparticles potentially can be suppressed to the electronic noise limit of the imaging system [71]. Qin *et al*. reported the gadolinium(III)-gold nanorods have been developed as a dual-modality probe for MRI and PAI to trace macrophages for determining the degree of inflammation [72].

Another recent advance in PAI is the use of carbon-containing materials. For example, single-walled carbon nanotubes (SWNTs) conjugated with cyclic Arg-Gly-Asp (RGD) peptides can be used as a contrast agent for PAI of tumors [73]. Intravenous administration of these targeted nanotubes to mice bearing tumors yielded 8-fold greater PA signal in the tumor than mice injected with non-targeted nanotubes. These results were verified *ex vivo* using Raman microscopy. Similarly, ICG dye–enhanced single walled carbon nanotubes (SWNT-ICG) were conjugated as the contrast agent with cyclic Arg-Gly-Asp (RGD) peptides to molecularly target the alpha(v)beta(3) integrins, which are associated with tumor angiogenesis [40]. Intravenous administration of this tumor-targeted contrast agent to tumor-bearing mice yielded significantly higher PA signal in the tumor than in mice injected with the untargeted contrast agent. The new contrast agent had 300-fold higher PA contrast in living tissues than previously reported SWNTs, equivalent to subnanomolar sensitivities. Qualitatively similar results were obtained with SWNTs that were coated with another dye, QSY (SWNT-QSY) [74]; those authors were able to spectrally separate the PA signals of SWNT-QSY and SWNT-ICG in living animals injected subcutaneously with both particles in the same location, raising the possibility of multiplexing *in vivo* studies. A related approach demonstrated that high-contrast and highly efficient targeting of alpha(v)beta(3) integrin–positive U87 human glioblastoma tumors in mice could be achieved [44]. This study also demonstrated the nontoxicity of functionalized SWNTs; this feature ensures that SWNTs can be used for clinical applications. The results suggest that PMI, in conjunction with antibody-functionalized SWNTs, potentially represents an efficient method of diagnosing early tumors. Overall, these findings indicate that PAI using targeted SWNTs may contribute to non-invasive cancer imaging and monitoring of nanotherapeutics in living subjects.

Further evidence regarding the *in vivo* behaviors and functions of SWNTs has been provided by microscopic studies, specifically by PAM. Multi-scale PAM was used to detect, map, and quantify trace amounts of SWNT in a variety of histological tissue specimens consisting of cancer and benign tissue biopsies [75]. Both optical-resolution and acoustic-resolution PAM allow the detection and quantification of SWNTs in histological specimens with scalable spatial resolution and depth penetration. The results demonstrate the potential of PAM as a promising imaging technique in histological specimens, and could complement the capabilities of current optical and electron microscopy techniques in the analysis of histological specimens containing SWNTs. Similar approaches could also be useful in the study of 3D polymeric scaffolds, which provide structural support and function as substrates for cells and bioactive molecules necessary for tissue regeneration; however, noninvasive real-time imaging of scaffolds and the process of tissue formation within the scaffold remains a challenge. Multiscale PAM, consisting of both

acoustic-resolution and optical-resolution PAM, was employed to image and characterize single-walled carbon-nanotube (SWNT)-incorporated poly(lactic-co-glycolic acid) polymer scaffolds immersed in biological buffer [76]. SWNTs were incorporated to reinforce the mechanical properties of the scaffolds, and to enhance the PA signal from the scaffolds. The results suggest that PAM is a promising tool for noninvasive real-time imaging and monitoring of tissue engineering scaffolds *in vitro*, and *in vivo* under physiological conditions.

In practical terms, as with the gold-containing agents described above, the nanocarbon-containing agents can be used to monitor sentinel lymph nodes (SLNs). As noted above, SWNTs have been used to map SLNs as well as the urinary bladder, demonstrating that dye-conjugated SWNTs might be used to identify SLNs in breast cancer patients [77]. Furthermore, non-invasive SWNT-enhanced PA identification of SLN has been reported in a rat model [78]. In that system, SLNs were successfully visualized *in vivo* by PA imaging with high contrast-to-noise ratio and resolution. The SWNTs also exhibited a wideband optical absorption, generating PA signals over an excitation wavelength range of 740–820 nm. Thus, by varying the incident light wavelength to the near infrared region, where biological tissues (hemoglobin, tissue pigments, lipids, and water) show low light absorption, the imaging depth can be maximized.

Finally, nanocarbon-containing particles might also be used to enhance stem-cell therapy, as revealed by a novel nanoparticle-enhanced biophysical technique that differentiates multipotent marrow stromal cells (MSCs) into osteoblasts [79]. To observe osteodifferentiation under PA stimulation, tissue culture plates were seeded with MSCs without the osteogenic culture supplements in the presence and absence of SWNTs and gold nanoparticles. The alkaline phosphatase activity, calcium content, and osteopontin secretion were monitored as indicators of MSC differentiation toward osteoblasts. The PA stimulated groups exhibited more than a 600% increase in calcium content compared to the controls cultured with osteogenic supplements. Among the PA-stimulated groups, MSCs incubated with SWNTs showed up to 97% greater calcium content than those that did not contain SWNTs. The results demonstrated that PA stimulation not only promotes osteogenesis but also is synergistically enhanced by the presence of nanoparticles and, thus, has major implications for bone regeneration applications.

PAI for Evaluating Therapy

Imaging techniques play a significant role in cancer therapy, from precise planning and guidance to evaluation of efficacy. In particular, PAI has demonstrated the potential to aid therapies by providing sequential monitoring of tumor functional properties, such as changes in tumor vasculature before, during, and after therapeutic procedures. The therapeutic agents used for photodynamic therapy (PDT) or photothermal therapy (PTT) can also act as PA contrast agents, owing to their high optical absorption properties in the NIR region (e.g., protoporphyrin IX for PDT and AuNRs for PTT) [42, 80].

PAI can also assist in determining the location of the tumor, gauging the heterogeneities in vasculature within the tumor, and observing heterogeneities in accumulation of therapeutic agents. For example, golden carbon nanotubes (AuNTs) conjugated with an antibody specific to the lymphatic endothelial hyaluronan receptor-1 have been used to visualize heterogeneities of endogenous low-absorbing mesenteric structures in nude mice [77]. In that study, the PA image provided information about the heterogeneous accumulation of targeted AuNTs and helped to guide PTT aimed at causing spatially specific thermal damage to the lymphatic walls

In addition, PAI can also aid in customized delivery of drugs using multi-functional nanoparticles. An example of such a nanoagent is a system consisting of a poly(lactic-*co*-glycolic acid) (PLGA) polymer core and an outer cage network made of silver. The outer silver cage enhances contrast in PAI, and the inner core of the nanosystem contains the drug doxorubicin. Initial studies indicated that such PLGA-based nanosystems have the potential to significantly increase contrast in PAI, while simultaneously delivering customized payloads of drug to tumor cells [81]. Another example of controlled and customized drug delivery involves light-triggered nano-constructs, e.g., microspheres containing the drug paclitaxel encapsulated in hollow gold nanospheres. Depending on the concentration of hollow gold nanospheres in the tumor, the light dose can be adjusted to allow optimal release of drug paclitaxel [82].

FUTURE PERSPECTIVES

By differentiating the optical properties of tissues, PAI is well suited to measure functional properties of tumors *in vivo*. For example, multi-wavelength PAI can

visualize vasculature and identify hypoxic conditions within tumors. Current functional imaging techniques suffer from poor spatial resolution or inadequate penetration depth. By contrast, PAI is non-ionizing and can image deep tissue structures with acceptable spatial resolution.

Nanosize contrast agents, such as gold, have distinct advantages in cancer therapy, starting with their inherent ability to accumulate at tumor sites due to the enhanced permeability and retention (EPR) effect. Although the further investigation into toxicity of nanomaterials and gold is necessary, their versatility provides opportunities for multifunctionalization and creation of "smart contrast agents". Contrast agents for PAI can be functionalized to achieve both diagnosis and treatment and they can be targeted to specific cells by the addition of surface ligands against specific receptors. Multifunctional and cell specific contrast agents have great potential for clinically translatable advances that can positively impact the overall process of cancer diagnosis and treatment, and result in enhanced quality of life for cancer patients. The most crucial aspect in future development of nano-based medicine will likely be the ability for multifunctionalization and successful engineering and fabrication of multimodal nanotheranostic designs. The ultimate goal will be to maximize the amount of diagnostic information and therapeutic efficacy and reduce the degree and frequency of invasive interventions.

Biomedical photoacoustics has seen tremendous growth in the past two decades, PAI research is still in progress. We predict that the next decade will bring rapid progress in the field of photoacoustics, ranging from instrumentation development, to regulatory approvals, to pre-clinical and clinical applications.

ACKNOWLEDGEMENTS

This work was supported by JST Collaborative Research Based on Industrial Demand (*In vivo* Molecular Imaging: Towards Biophotonics Innovations in Medicine).

REFERENCES

[1] Histed SN, Lindenberg ML, Mena E, Turkbey B, Choyke PL, Kurdziel KA. Review of functional/anatomical imaging in oncology. Nucl Med Commun 2012; 33: 349-61. http://dx.doi.org/10.1097/MNM.0b013e32834ec8a5

[2] Kircher MF, Willmann JK. Molecular body imaging: MR imaging, CT, and US. part I. principles. Radiology 2012; 263: 633-43. http://dx.doi.org/10.1148/radiol.12102394

[3] Roach M, 3rd, Alberini JL, Pecking AP, Testori A, Verrecchia F, Soteldo J, *et al.* Diagnostic and therapeutic imaging for cancer: therapeutic considerations and future directions. J Surg Oncol 2011; 103: 587-601. http://dx.doi.org/10.1002/jso.21805

[4] Frangioni JV. New technologies for human cancer imaging. J Clin Oncol 2008; 26: 4012-21. http://dx.doi.org/10.1200/JCO.2007.14.3065

[5] Mallidi S, Luke GP, Emelianov S. Photoacoustic imaging in cancer detection, diagnosis, and treatment guidance. Trends Biotechnol 2011; 29: 213-21. http://dx.doi.org/10.1016/j.tibtech.2011.01.006

[6] Zhang HF, Maslov K, Stoica G, Wang LV. Functional photoacoustic microscopy for high-resolution and noninvasive *in vivo* imaging. Nat Biotechnol 2006; 24: 848-51. http://dx.doi.org/10.1038/nbt1220

[7] Siphanto RI, Thumma KK, Kolkman RG, van Leeuwen TG, de Mul FF, van Neck JW, *et al.* Serial noninvasive photoacoustic imaging of neovascularization in tumor angiogenesis. Opt Express 2005; 13: 89-95. http://dx.doi.org/10.1364/OPEX.13.000089

[8] Wang LV, Hu S. Photoacoustic tomography: *in vivo* imaging from organelles to organs. Science 2012; 335: 1458-62. http://dx.doi.org/10.1126/science.1216210

[9] Wang LV. Multiscale photoacoustic microscopy and computed tomography. Nat Photonics 2009; 3: 503-9. http://dx.doi.org/10.1038/nphoton.2009.157

[10] Emelianov SY, Li PC, O'Donnell M. Photoacoustics for molecular imaging and therapy. Phys Today 2009; 62: 34-9. http://dx.doi.org/10.1063/1.3141939

[11] Staley J, Grogan P, Samadi AK, Cui H, Cohen MS, Yang X. Growth of melanoma brain tumors monitored by photoacoustic microscopy. J Biomed Opt 2010; 15: 040510. http://dx.doi.org/10.1117/1.3478309

[12] Oh JT, Li ML, Zhang HF, Maslov K, Stoica G, Wang LV. Three-dimensional imaging of skin melanoma *in vivo* by dual-wavelength photoacoustic microscopy. J Biomed Opt 2006; 11: 34032. http://dx.doi.org/10.1117/1.2210907

[13] Weight RM, Viator JA, Dale PS, Caldwell CW, Lisle AE. Photoacoustic detection of metastatic melanoma cells in the human circulatory system. Opt Lett 2006; 31: 2998-3000. http://dx.doi.org/10.1364/OL.31.002998

[14] McCormack D, Al-Shaer M, Goldschmidt BS, Dale PS, Henry C, Papageorgio C, *et al.* Photoacoustic detection of melanoma micrometastasis in sentinel lymph nodes. J Biomech Eng 2009; 131: 074519. http://dx.doi.org/10.1115/1.3169247

[15] Zhang C, Maslov K, Wang LV. Subwavelength-resolution label-free photoacoustic microscopy of optical absorption *in vivo*. Opt Lett 2010; 35: 3195-7. http://dx.doi.org/10.1364/OL.35.003195

[16] Zhang Y, Cai X, Choi SW, Kim C, Wang LV, Xia Y. Chronic label-free volumetric photoacoustic microscopy of melanoma cells in three-dimensional porous scaffolds. Biomaterials 2010; 31: 8651-8. http://dx.doi.org/10.1016/j.biomaterials.2010.07.089

[17] Jose J, Grootendorst DJ, Vijn TW, Wouters MW, van Boven H, van Leeuwen TG, *et al.* Initial results of imaging melanoma metastasis in resected human lymph nodes using photoacoustic computed tomography. J Biomed Opt 2011; 16: 096021. http://dx.doi.org/10.1117/1.3631705

[18] Grootendorst DJ, Jose J, Wouters MW, van Boven H, Van der Hage J, Van Leeuwen TG, *et al.* First experiences of photoacoustic imaging for detection of melanoma metastases in resected human lymph nodes. Lasers Surg Med 2012; 44: 541-9. http://dx.doi.org/10.1002/lsm.22058

[19] Hu S, Maslov K, Wang LV. Second-generation optical-resolution photoacoustic microscopy with improved sensitivity and speed. Opt Lett 2011; 36: 1134-6. http://dx.doi.org/10.1364/OL.36.001134

[20] Lao Y, Xing D, Yang S, Xiang L. Noninvasive photoacoustic imaging of the developing vasculature during early tumor growth. Phys Med Biol 2008; 53: 4203-12. http://dx.doi.org/10.1088/0031-9155/53/15/013

[21] Hu S, Wang LV. Photoacoustic imaging and characterization of the microvasculature. J Biomed Opt 2010; 15: 011101. http://dx.doi.org/10.1117/1.3281673

[22] Wang X, Roberts WW, Carson PL, Wood DP, Fowlkes JB. Photoacoustic tomography: a potential new tool for prostate cancer. Biomed Opt Express 2010; 1: 1117-26. http://dx.doi.org/10.1364/BOE.1.001117

[23] Heijblom M, Klaase JM, van den Engh FM, van Leeuwen TG, Steenbergen W, Manohar S. Imaging tumor vascularization for detection and diagnosis of breast cancer. Technol Cancer Res Treat 2011; 10: 607-23.

[24] Yao J, Maslov KI, Zhang Y, Xia Y, Wang LV. Label-free oxygen-metabolic photoacoustic microscopy *in vivo*. J Biomed Opt 2011; 16: 076003. http://dx.doi.org/10.1117/1.3594786

[25] Kitai T, Torii M, Sugie T, Kanao S, Mikami Y, Shiina T, *et al.* Photoacoustic mammography: initial clinical results. Breast Cancer 2012. http://dx.doi.org/10.1007/s12282-012-0363-0

[26] Turkbey B, Kobayashi H, Ogawa M, Bernardo M, Choyke PL. Imaging of tumor angiogenesis: functional or targeted? AJR Am J Roentgenol 2009; 193: 304-13. http://dx.doi.org/10.2214/AJR.09.2869

[27] Lungu GF, Li ML, Xie X, Wang LV, Stoica G. *In vivo* imaging and characterization of hypoxia-induced neovascularization and tumor invasion. Int J Oncol 2007; 30: 45-54.

[28] Li M-L, Oh J-T, Xie X, Ku G, Wang W, Li C, *et al.* Simultaneous molecular and hypoxia imaging of brain tumors *in vivo* using spectroscopic photoacoustic tomography. Proceedings of the IEEE 2008; 96: 481-9. http://dx.doi.org/10.1109/JPROC.2007.913515

[29] Razansky D, Vinegoni C, Ntziachristos V. Multispectral photoacoustic imaging of fluorochromes in small animals. Opt Lett 2007; 32: 2891-3. http://dx.doi.org/10.1364/OL.32.002891

[30] Bhattacharyya S, Wang S, Reinecke D, Kiser W, Jr., Kruger RA, DeGrado TR. Synthesis and evaluation of near-infrared (NIR) dye-herceptin conjugates as photoacoustic computed tomography (PCT) probes for HER2 expression in breast cancer. Bioconjug Chem 2008; 19: 1186-93. http://dx.doi.org/10.1021/bc700482u

[31] Ku G, Wang LV. Deeply penetrating photoacoustic tomography in biological tissues enhanced with an optical contrast agent. Opt Lett 2005; 30: 507-9. http://dx.doi.org/10.1364/OL.30.000507

[32] Kim G, Huang SW, Day KC, O'Donnell M, Agayan RR, Day MA, *et al.* Indocyanine-green-embedded PEBBLEs as a contrast agent for photoacoustic imaging. J Biomed Opt 2007; 12: 044020. http://dx.doi.org/10.1117/1.2771530

[33] Kim C, Song KH, Gao F, Wang LV. Sentinel lymph nodes and lymphatic vessels: noninvasive dual-modality *in vivo* mapping by using indocyanine green in rats--volumetric spectroscopic photoacoustic imaging and planar fluorescence imaging. Radiology 2010; 255: 442-50. http://dx.doi.org/10.1148/radiol.10090281

[34] Kohl Y, Kaiser C, Bost W, Stracke F, Thielecke H, Wischke C, *et al.* Near-infrared dye-loaded PLGA nanoparticles prepared by spray drying for photoacoustic applications. Int J Artif Organs 2011; 34: 249-52. http://dx.doi.org/10.5301/IJAO.2011.6405

[35] Rajian JR, Fabiilli ML, Fowlkes JB, Carson PL, Wang X. Drug delivery monitoring by photoacoustic tomography with an ICG encapsulated double emulsion. Opt Express 2011; 19: 14335-47. http://dx.doi.org/10.1364/OE.19.014335

[36] Koo J, Jeon M, Oh Y, Kang HW, Kim J, Kim C, *et al. In vivo* non-ionizing photoacoustic mapping of sentinel lymph nodes and bladders with ICG-enhanced carbon nanotubes. Phys Med Biol 2012; 57: 7853-62. http://dx.doi.org/10.1088/0031-9155/57/23/7853

[37] Wang B, Zhao Q, Barkey NM, Morse DL, Jiang H. Photoacoustic tomography and fluorescence molecular tomography: a comparative study based on indocyanine green. Med Phys 2012; 39: 2512-7. http://dx.doi.org/10.1118/1.3700401

[38] Levi J, Kothapalli SR, Ma TJ, Hartman K, Khuri-Yakub BT, Gambhir SS. Design, synthesis, and imaging of an activatable photoacoustic probe. J Am Chem Soc 2010; 132: 11264-9. http://dx.doi.org/10.1021/ja104000a

[39] Yang S, Ye F, Xing D. Intracellular label-free gold nanorods imaging with photoacoustic microscopy. Opt Express 2012; 20: 10370-5. http://dx.doi.org/10.1364/OE.20.010370

[40] de la Zerda A, Liu Z, Bodapati S, Teed R, Vaithilingam S, Khuri-Yakub BT, *et al.* Ultrahigh sensitivity carbon nanotube agents for photoacoustic molecular imaging in living mice. Nano Lett 2010; 10: 2168-72. http://dx.doi.org/10.1021/nl100890d

[41] Kim C, Cho EC, Chen J, Song KH, Au L, Favazza C, *et al. In vivo* molecular photoacoustic tomography of melanomas targeted by bioconjugated gold nanocages. ACS Nano 2010; 4: 4559-64. http://dx.doi.org/10.1021/nn100736c

[42] Li PC, Wang CR, Shieh DB, Wei CW, Liao CK, Poe C, *et al. In vivo* photoacoustic molecular imaging with simultaneous multiple selective targeting using antibody-conjugated gold nanorods. Opt Express 2008; 16: 18605-15. http://dx.doi.org/10.1364/OE.16.018605

[43] Mallidi S, Larson T, Tam J, Joshi PP, Karpiouk A, Sokolov K, *et al.* Multiwavelength photoacoustic imaging and plasmon resonance coupling of gold nanoparticles for selective detection of cancer. Nano Lett 2009; 9: 2825-31. http://dx.doi.org/10.1021/nl802929u

[44] Xiang L, Yuan Y, Xing D, Ou Z, Yang S, Zhou F. Photoacoustic molecular imaging with antibody-functionalized single-walled carbon nanotubes for early diagnosis of tumor. J Biomed Opt 2009; 14: 021008. http://dx.doi.org/10.1117/1.3078809

[45] Zhang Q, Iwakuma N, Sharma P, Moudgil BM, Wu C, McNeill J, *et al.* Gold nanoparticles as a contrast agent for *in vivo* tumor imaging with photoacoustic tomography. Nanotechnology 2009; 20: 395102. http://dx.doi.org/10.1088/0957-4484/20/39/395102

[46] Shashkov EV, Everts M, Galanzha EI, Zharov VP. Quantum dots as multimodal photoacoustic and photothermal contrast agents. Nano Lett 2008; 8: 3953-8. http://dx.doi.org/10.1021/nl802442x

[47] Mallidi S, Larson T, Aaron J, Sokolov K, Emelianov S. Molecular specific optoacoustic imaging with plasmonic nanoparticles. Opt Express 2007; 15: 6583-8. http://dx.doi.org/10.1364/OE.15.006583

[48] Ha S, Carson A, Agarwal A, Kotov NA, Kim K. Detection and monitoring of the multiple inflammatory responses by photoacoustic molecular imaging using selectively targeted gold nanorods. Biomed Opt Express 2011; 2: 645-57. http://dx.doi.org/10.1364/BOE.2.000645

[49] Wang B, Yantsen E, Larson T, Karpiouk AB, Sethuraman S, Su JL, *et al.* Plasmonic intravascular photoacoustic imaging

for detection of macrophages in atherosclerotic plaques. Nano Lett 2009; 9: 2212-7. http://dx.doi.org/10.1021/nl801852e

[50] Yeager D, Karpiouk A, Wang B, Amirian J, Sokolov K, Smalling R, *et al.* Intravascular photoacoustic imaging of exogenously labeled atherosclerotic plaque through luminal blood. J Biomed Opt 2012; 17: 106016. http://dx.doi.org/10.1117/1.JBO.17.10.106016

[51] Rouleau L, Berti R, Ng VW, Matteau-Pelletier C, Lam T, Sabourd P, *et al.* VCAM-1-targeting gold nanoshell probe for photoacoustic imaging of atherosclerotic plaque in mice. Contrast Media Mol Imaging 2013; 8: 27-39.

[52] Song KH, Kim C, Cobley CM, Xia Y, Wang LV. Near-infrared gold nanocages as a new class of tracers for photoacoustic sentinel lymph node mapping on a rat model. Nano Lett 2009; 9: 183-8. http://dx.doi.org/10.1021/nl802746w

[53] Cai X, Li W, Kim CH, Yuan Y, Wang LV, Xia Y. *In vivo* quantitative evaluation of the transport kinetics of gold nanocages in a lymphatic system by noninvasive photoacoustic tomography. ACS Nano 2011; 5: 9658-67. http://dx.doi.org/10.1021/nn203124x

[54] Pan D, Pramanik M, Senpan A, Ghosh S, Wickline SA, Wang LV, *et al.* Near infrared photoacoustic detection of sentinel lymph nodes with gold nanobeacons. Biomaterials 2010; 31: 4088-93. http://dx.doi.org/10.1016/j.biomaterials.2010.01.136

[55] Lu W, Melancon MP, Xiong C, Huang Q, Elliott A, Song S, *et al.* Effects of photoacoustic imaging and photothermal ablation therapy mediated by targeted hollow gold nanospheres in an orthotopic mouse xenograft model of glioma. Cancer Res 2011; 71: 6116-21. http://dx.doi.org/10.1158/0008-5472.CAN-10-4557

[56] Lu W, Huang Q, Ku G, Wen X, Zhou M, Guzatov D, *et al.* Photoacoustic imaging of living mouse brain vasculature using hollow gold nanospheres. Biomaterials 2010; 31: 2617-26. http://dx.doi.org/10.1016/j.biomaterials.2009.12.007

[57] Cui H, Yang X. *In vivo* imaging and treatment of solid tumor using integrated photoacoustic imaging and high intensity focused ultrasound system. Med Phys 2010; 37: 4777-81. http://dx.doi.org/10.1118/1.3480963

[58] Moon GD, Choi SW, Cai X, Li W, Cho EC, Jeong U, *et al.* A new theranostic system based on gold nanocages and phase-change materials with unique features for photoacoustic imaging and controlled release. J Am Chem Soc 2011; 133: 4762-5. http://dx.doi.org/10.1021/ja200894u

[59] Wang PH, Liu HL, Hsu PH, Lin CY, Wang CR, Chen PY, *et al.* Gold-nanorod contrast-enhanced photoacoustic micro-imaging of focused-ultrasound induced blood-brain-barrier opening in a rat model. J Biomed Opt 2012; 17: 061222. http://dx.doi.org/10.1117/1.JBO.17.6.061222

[60] Chen LC, Wei CW, Souris JS, Cheng SH, Chen CT, Yang CS, *et al.* Enhanced photoacoustic stability of gold nanorods by silica matrix confinement. J Biomed Opt 2010; 15: 016010. http://dx.doi.org/10.1117/1.3292574

[61] Bayer CL, Chen YS, Kim S, Mallidi S, Sokolov K, Emelianov S. Multiplex photoacoustic molecular imaging using targeted silica-coated gold nanorods. Biomed Opt Express 2011; 2: 1828-35. http://dx.doi.org/10.1364/BOE.2.001828

[62] Chen YS, Frey W, Kim S, Kruizinga P, Homan K, Emelianov S. Silica-coated gold nanorods as photoacoustic signal nanoamplifiers. Nano Lett 2011; 11: 348-54. http://dx.doi.org/10.1021/nl1042006

[63] Bayer CL, Nam SY, Chen YS, Emelianov SY. Photoacoustic signal amplification through plasmonic nanoparticle aggregation. J Biomed Opt 2013; 18: 16001. http://dx.doi.org/10.1117/1.JBO.18.1.016001

[64] Pan D, Pramanik M, Senpan A, Wickline SA, Wang LV, Lanza GM. A facile synthesis of novel self-assembled gold nanorods designed for near-infrared imaging. J Nanosci Nanotechnol 2010; 10: 8118-23. http://dx.doi.org/10.1166/jnn.2010.3034

[65] Zhang B, Fang CY, Chang CC, Peterson R, Maswadi S, Glickman RD, *et al.* Photoacoustic emission from fluorescent nanodiamonds enhanced with gold nanoparticles. Biomed Opt Express 2012; 3: 1662-29. http://dx.doi.org/10.1364/BOE.3.001662

[66] Kim S, Chen YS, Luke GP, Emelianov SY. *In vivo* three-dimensional spectroscopic photoacoustic imaging for monitoring nanoparticle delivery. Biomed Opt Express 2011; 2: 2540-50. http://dx.doi.org/10.1364/BOE.2.002540

[67] Fournelle M, Bost W, Tarner IH, Lehmberg T, Weiss E, Lemor R, *et al.* Antitumor necrosis factor-alpha antibody-coupled gold nanorods as nanoprobes for molecular optoacoustic imaging in arthritis. Nanomedicine 2012; 8: 346-54. http://dx.doi.org/10.1016/j.nano.2011.06.020

[68] Jokerst JV, Cole AJ, Van de Sompel D, Gambhir SS. Gold Nanorods for Ovarian Cancer Detection with Photoacoustic Imaging and Resection Guidance *via* Raman Imaging in Living Mice. ACS Nano 2012; 6: 10366-77. http://dx.doi.org/10.1021/nn304347g

[69] Jokerst JV, Thangaraj M, Kempen PJ, Sinclair R, Gambhir SS. Photoacoustic imaging of mesenchymal stem cells in living mice *via* silica-coated gold nanorods. ACS Nano 2012; 6: 5920-30. http://dx.doi.org/10.1021/nn302042y

[70] Nam SY, Ricles LM, Suggs LJ, Emelianov SY. *In vivo* ultrasound and photoacoustic monitoring of mesenchymal stem cells labeled with gold nanotracers. PLoS One 2012; 7: e37267. http://dx.doi.org/10.1371/journal.pone.0037267

[71] Jin Y, Jia C, Huang SW, O'Donnell M, Gao X. Multifunctional nanoparticles as coupled contrast agents. Nat Commun 2010; 1: 41. http://dx.doi.org/10.1038/ncomms1042

[72] Qin H, Zhou T, Yang S, Chen Q, Xing D. Gadolinium(III)-gold nanorods for MRI and photoacoustic imaging dual-modality detection of macrophages in atherosclerotic inflammation. Nanomedicine (Lond) 2013; in press. http://dx.doi.org/10.2217/nnm.12.168

[73] De la Zerda A, Zavaleta C, Keren S, Vaithilingam S, Bodapati S, Liu Z, *et al.* Carbon nanotubes as photoacoustic molecular imaging agents in living mice. Nat Nanotechnol 2008; 3: 557-62. http://dx.doi.org/10.1038/nnano.2008.231

[74] de la Zerda A, Bodapati S, Teed R, May SY, Tabakman SM, Liu Z, *et al.* Family of enhanced photoacoustic imaging agents for high-sensitivity and multiplexing studies in living mice. ACS Nano 2012; 6: 4694-701. http://dx.doi.org/10.1021/nn204352r

[75] Avti PK, Hu S, Favazza C, Mikos AG, Jansen JA, Shroyer KR, *et al.* Detection, mapping, and quantification of single walled carbon nanotubes in histological specimens with photoacoustic microscopy. PLoS One 2012; 7: e35064. http://dx.doi.org/10.1371/journal.pone.0035064

[76] Cai X, Paratala BS, Hu S, Sitharaman B, Wang LV. Multiscale photoacoustic microscopy of single-walled carbon nanotube-incorporated tissue engineering scaffolds. Tissue Eng Part C Methods 2012; 18: 310-7. http://dx.doi.org/10.1089/ten.tec.2011.0519

[77] Kim JW, Galanzha EI, Shashkov EV, Moon HM, Zharov VP. Golden carbon nanotubes as multimodal photoacoustic and photothermal high-contrast molecular agents. Nat Nanotechnol 2009; 4: 688-94. http://dx.doi.org/10.1038/nnano.2009.231

[78] Pramanik M, Song KH, Swierczewska M, Green D, Sitharaman B, Wang LV. *In vivo* carbon nanotube-enhanced non-invasive photoacoustic mapping of the sentinel lymph node. Phys Med Biol 2009; 54: 3291-301. http://dx.doi.org/10.1088/0031-9155/54/11/001

[79] Green DE, Longtin JP, Sitharaman B. The effect of nanoparticle-enhanced photoacoustic stimulation on multipotent marrow stromal cells. ACS Nano 2009; 3: 2065-72. http://dx.doi.org/10.1021/nn900434p

[80] Xiang L, Xing D, Gu H, Yang D, Yang S, Zeng L, *et al.* Real-time optoacoustic monitoring of vascular damage during photodynamic therapy treatment of tumor. J Biomed Opt 2007; 12: 014001. http://dx.doi.org/10.1117/1.2437752

[81] Homan K, Shah J, Gomez S, Gensler H, Karpiouk A, Brannon-Peppas L, *et al.* Silver nanosystems for photoacoustic imaging and image-guided therapy. J Biomed Opt 2010; 15: 021316. http://dx.doi.org/10.1117/1.3365937

[82] You J, Shao R, Wei X, Gupta S, Li C. Near-infrared light triggers release of Paclitaxel from biodegradable microspheres: photothermal effect and enhanced antitumor activity. Small 2010; 6: 1022-31. http://dx.doi.org/10.1002/smll.201000028

Received on 01-02-2013 Accepted on 22-03-2013 Published on 30-04-2013

http://dx.doi.org/10.6000/1927-7229.2013.02.02.5